Helvetica Chimica Acta

HELVETICA chimica acta

RESEARCH ARTICLE OPEN ACCESS

A Compact Circularly Polarized Luminescence Emitter–Chirality of a [2.2]-Paracyclophane Macrocycle

Salome L. Heim[1] | Adriano D'Addio[2] | Olaf Fuhr[3,4] | Dieter Fenske[3,4,5] | Marcel Mayor[1,4,5]

[1]University of Basel, Basel, Switzerland | [2]University of Copenhagen, Copenhagen, Denmark | [3]Karlsruhe Nano Micro Facility (KNMFi), Karlsruhe Institute of Technology (KIT), Karlsruhe, Germany | [4]Institute For Nanotechnology (INT), Karlsruhe Institute of Technology (KIT), Karlsruhe, Germany | [5]Lehn Institute of Functional Materials, School of Chemistry, Sun Yat-Sen University, Guangzhou, P. R. China

Correspondence: Marcel Mayor (marcel.mayor@unibas.ch)

Received: 22 January 2026 | **Revised:** 21 April 2026 | **Accepted:** 29 April 2026

Keywords: [2.2]Paracyclophane | circularly polarized luminescence | electronic circular dichroism | helical chirality | planar chirality

ABSTRACT

Chiral organic molecules with pronounced chiroptical responses are of significant interest for applications ranging from bioimaging to optoelectronic devices. Herein, we report comprehensive chiroptical investigations of a compact [2.2]paracyclophane (PCP)-based macrocycle and its open precursor. While the synthesis of the structure was reported by the group of Michael Haley, chiroptical investigations were still missing. The rigid PCP core acts as a chiral template, inducing helical twisting within the conjugated diacetylene framework. Owing to its low atomic count, the compact macrocycle represents an attractive model system for combined experimental and computational studies, enabling fast DFT and TD-DFT calculations. The macrocycle and its open synthetic precursor were synthesized, structurally characterized, and, in both cases, enantiomers were separated on a chiral stationary phase HPLC. Absolute configurations were assigned through TD-DFT calculations. Optical measurements reveal enhanced conjugation and redshifted emission upon macrocyclization. Electric circular dichroism (ECD) spectra exhibit multiple intense cotton bands. Both macrocycle and open precursor display exceptionally high circularly polarized luminescence (CPL) dissymmetry factors, with glum around 10^{-2}. Despite moderate CPL brightness, limited by the compounds' quantum yields, these results demonstrate the strong chiral amplification imparted by the PCP. The presented scaffold provides a versatile platform for probing structure–property relationships in chiral conjugated macrocycles.

1 | Introduction

Our group has maintained a long-standing interest in the synthesis and study of chiral organic molecules. This work has encompassed the synthesis and chiroptical analysis of curved aromatics [1, 2], trinorbornane derivatives [3, 4], chiral nanobelts [5], Geländer molecules [6–15], and cross-shaped monomers designed for polymerizations [16, 17]. More recently, we have also focused on incorporating [2.2]paracyclophane (PCP) into macrocyclic architectures as a strategy to efficiently introduce chirality into organic frameworks [18–21]. PCP derivatives are particularly attractive due to their pronounced chiroptical responses and high barriers to isomerization.

The compact macrocycle **1** (Figure 1 and Scheme 1), first synthesized by the group of Michael Haley, represents a compelling example within this context: the PCP core with its *pseudo-ortho* substitution pattern (Figure 1 in magenta) functions as a rigid chiral subunit that induces a helical twist on its 1,4-diphenylbuta-1,3-diyne backbone (Figure 1, in orange) [22, 23].

Dedicated to the 125th anniversary of the Swiss Chemical Society, recognizing their outstanding engagement for the community.

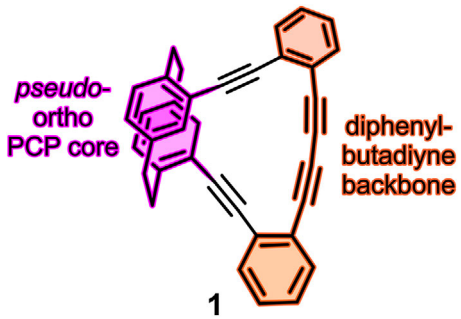

FIGURE 1 | Structure and functional subunits of the macrocycle **1**. In the displayed enantiomer (P)-1, the planar chiral *pseudo-ortho* PCP subunit with its (R_p) configuration forces the macrocycle into a (*P*) helical chiral arrangement.

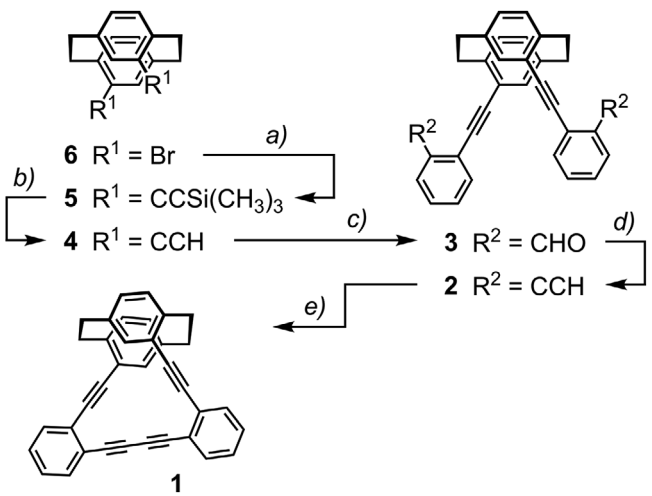

SCHEME 1 | Synthesis of the macrocycle **1**. Reagents and conditions: (a) TMS-acetylene, $Pd_2(dba)_3$, [(*t*-Bu)3PH]BF4, CuI, THF/TEA(1:1), 50°C, 1 h, 73%. (b) K_2CO_3, $MeOH/CH_2Cl_2$, (1:1), rt, 24 h, 73%. (c) *ortho*-bromobenzaldehyde, $Pd(PPh_3)_2Cl_2$, PPh_3, CuI, THF/TEA (4:1), 39%. (d) $CH_3COCN_2PO(OCH_3)_2$, Cs_2CO_3, MeOH/THF (1:1), 50°C, 10 min, 77%. (e) $Cu(OAc)_2.H_2O$, pyridine, 80°C, 1 h, 77%. While only the (*P*) enantiomer of **1** is displayed for clarity, the synthesis has been performed with the racemic mixture.

These types of electron-rich, chiral architectures are promising candidates for exhibiting intense chiroptical responses, such as strong electric circular dichroism (ECD) signals and/or circularly polarized luminescence (CPL) features, with potential applications in bioimaging, OLED technologies, and related areas [24–26]. Chiroptical data from closely related systems suggest that both expansion to a bicyclic system [27] and the introduction of electron-donating groups [28] are effective strategies for achieving high g_{lum} values.

In this work, the potential of the compact purely carbohydrate macrocycle **1** as a synthetically accessible and structurally compact model system with pronounced chiroptical properties is reported. The relatively low atomic count allows for efficient computational analysis, enabling rapid structure optimization via density functional theory (DFT) and time-dependent DFT (TD-DFT) calculations.

2 | Results and Discussion

2.1 | Synthesis

The assembly of the macrocycle **1** is displayed in Scheme 1. Starting with the literature-known racemic *pseudo-para* dibromo PCP, which can be thermally interconverted to its structural *pseudo-ortho* isomer **6** in a yield of 77% by heating it to 200°C in *ortho*-dichlorobenzene in a microwave reactor. Both bromines were first substituted by trimethylsilyl (TMS) protected acetylenes in a Sonogashira reaction. Thus, **6** was reacted with trimethylsilylacetylene with an in situ formed $Pd(P(t\text{-}Bu)_3)_4$ catalyst in the presence of CuI at 50°C to give **5** in a yield of 73% [29]. The reaction was completed after 1 h. Increasing the temperature led to a significant amount of side products, possibly due to deprotection of the TMS acetylene and subsequent engagement of the liberated ethynyl in further coupling reactions.

In the next step **5** was treated with Cs_2CO_3 in a $MeOH/CH_2Cl_2$ mixture at room temperature to give the deprotected diacetylene **4** in a yield of 73% after column chromatography. Although ^{13}C-NMR analysis shows a visible impurity in the aromatic region, the compound was used for the next step without further purification. Sonogashira cross-coupling of **4** with commercially available *ortho*-bromobenzaldehyde gave **3** in a yield of 39% after tedious purification steps. In particular, the separation from remaining phosphine ligands turned out to be challenging. In a homologation reaction, dialdehyde **3** was treated with the Ohira–Bestmann reagent at 50°C to give diacetylene macrocyclization precursor **2** in good yield of 77%. In a final step, the intramolecular ring closure was achieved by an oxidative homocoupling using $Cu(OAc)_2{\cdot}H_2O$ in pyridine at 80°C for 1 h to give **1** in 77% yield. The reaction was stirred for 1 h to ensure complete conversion. Closer inspection of the ring-closing experiment in subsequent repetitions with systematic variations displayed completion within a few minutes and independence of the yield from the concentration of the reaction. It seems that the spatial preorganization of the ethynyl groups in **2** clearly favors the intramolecular ring-closing over intermolecular oligomerization.

All compounds were characterized by ^{1}H-NMR, ^{13}C-NMR spectroscopy as well as high-resolution mass spectrometry (HRMS). Enantiopure samples of both the precursor **2** and macrocycle **1** were obtained by HPLC with a chiral stationary phase. Both compounds were baseline-separated into their enantiomers on Chiralpak IBN-5 as the stationary phase. For the macrocycle **1**, a variety of solvent mixtures were screened, and best results were obtained for a 4:1 heptane/isopropanol solvent ratio. For the precursor **2**, a 9:1 heptane/ethyl acetate mixture allowed the separation into its enantiomers. In both cases, the (*P*)-enantiomer eluted first.

2.2 | Optical Investigations

UV–vis and fluorescence spectra of racemic samples of both **1** and **2** are displayed in Figure 2. The comparison of both absorption spectra displays a pronounced increase in the intensity of the most prominent absorption band as well as a bathochromic shift of the highest absorption wavelength when going from the open

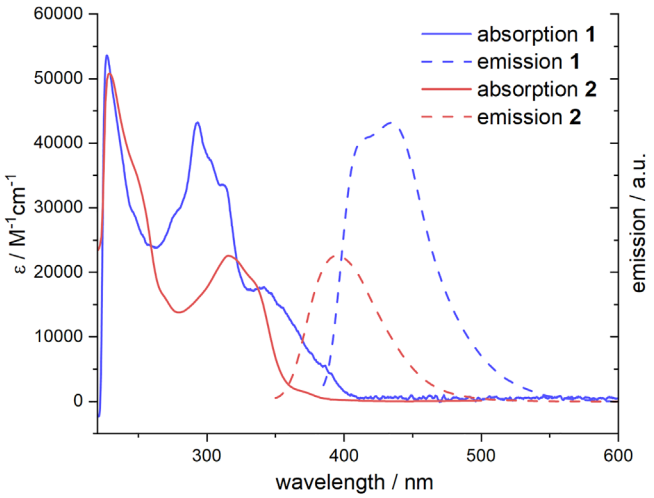

FIGURE 2 | Absorption (solid-line) and emission (dashed-line) spectra of racemic samples of **1** (blue) and **2** (red) recorded in CH_2Cl_2.

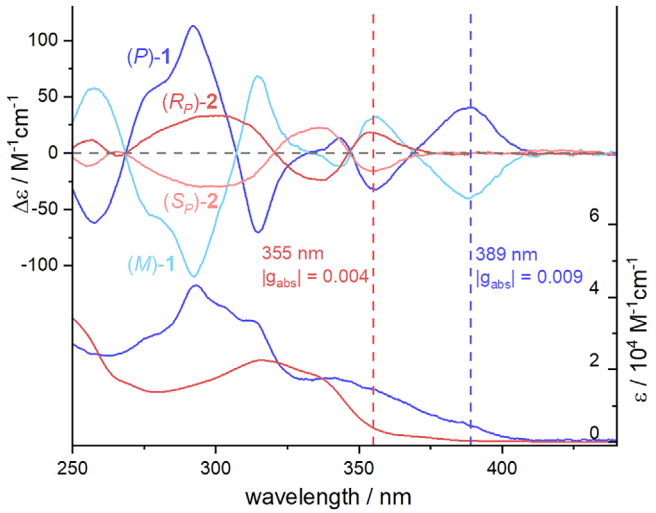

FIGURE 3 | ECD spectra of the macrocycles (*P*)-**1** and (*M*)-**1** in dark and light blue, respectively, and of their open precursors (R_P)-**2** and (S_P)-**2** in dark and light red, respectively, recorded as CH_2Cl_2 solutions. Corresponding absorption spectra of **1** (blue) and of **2** (red) are displayed on the right axis.

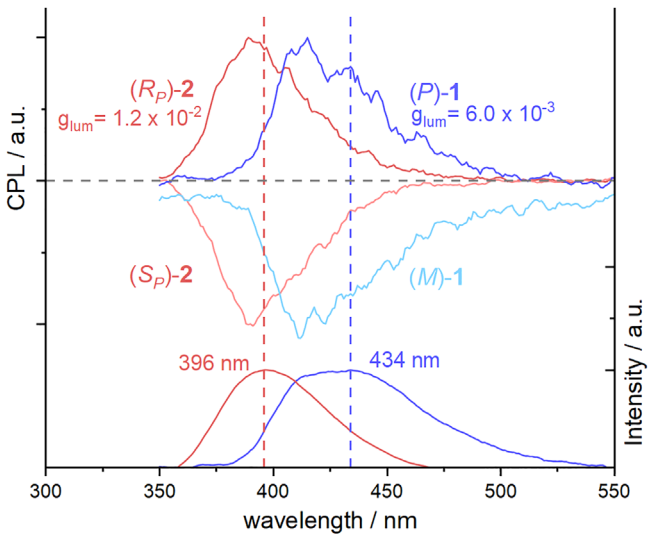

FIGURE 4 | CPL signals of (*P*)-**1** and (*M*)-**1** in dark and light blue, respectively, and of their open precursors (R_P)-**2** and (S_P)-**2** in dark and light red, respectively. On the right axis: luminescence intensity in blue for **1** and in red for **2**. Recorded at 0.1 transmission in CH_2Cl_2.

precursor **2** to macrocycle **1**. While the extinction coefficient of **1** in CH_2Cl_2 was determined to be 43 188 $M^{-1}cm^{-1}$ at 293 nm, that of **2** reaches only 22 579 $M^{-1}cm^{-1}$ at 316 nm. The behavior is rationalized by the increased conjugation after fusion of both chromophoric subunits. A similar behavior is also observed in the compounds' emission spectra. A distinct redshift together with an increased Stokes shift is observed from **2** to **1**. Quantum yields of both molecules in CH_2Cl_2 were measured and revealed a significant difference of 7% for **1** and 13% for **2**. The open form's higher quantum yield is consistent with the energy gap law, where the lower-energy emission of **1** is more susceptible to nonradiative decay relative to **2**. This remains surprising, however, as the open form's higher degrees of freedom would be expected to display reduced quantum yield due to additional vibrational relaxation pathways.

The ECD spectra of **1** and **2** in CH_2Cl_2 are displayed in Figure 3. Both molecules are characterized by a large number of distinct features and Cotton bands, indicating the presence of numerous underlying absorption transitions. Similar to their UV–vis spectra, the macrocycle **1** also exhibits stronger ECD signals almost over the entire spectral range compared to the open precursor **2**. Furthermore, an ECD signal above 370 nm was exclusively observed for **1**. The averaged g_{abs} of both enantiomers of **2** at 355 nm displays a value of $4{\cdot}10^{-3}$ and in case of **1** $9{\cdot}10^{-3}$ was observed (Figure 3), indicating higher dissymmetry of **1** in the ground state upon ring closing.

To assign the absolute configurations of the enantiomers of **1**, the recorded ECD spectra were compared with the simulated spectra of (*P*)-**1** applying TD-DFT calculations at the B3LYP/def2-TZVP level of theory using Orca 6.0 (Figure S6) [30–32]. The good match between the ECD spectra of the first eluting enantiomer and the simulated spectra suggested this to be *(P)*-**1** and the second eluting enantiomer to be *(M)*-**1**. While the enantiomer assignment of the macrocycle **1** was clear, the approach was less successful for the open precursor **2**. The increased flexibility of the structure with higher degrees of freedom made the search for the most favored arrangement challenging. The absolute configuration of **2** was thus assigned by converting an enantiopure sample to the closed macrocycle **1**. For that purpose, the first eluting sample of **2** was exposed to the ring-closing conditions e) displayed in Scheme 1. The ECD spectrum of the obtained macrocycle unambiguously allowed its identification as (*P*)-**1**, comprising the PCP subunit of (S_P) planar chirality (Figure 1). Consequently, the first eluting enantiomer of **2** was determined to be (S_P)-**2** and the second eluting (R_P)-**2**. Note that the open precursor **2** exhibits only planar chirality and that the helical chirality of **1** emerges upon formation of the macrocycle.

In order to characterize the excited state chirality, the CPL spectra of (*M*)-**1**, (*P*)-**1**, (S_P)-**2**, and (R_P)-**2** were recorded (Figure 4). Both molecules reach maxima near 10^{-2}, exceptionally high values for

TABLE 1 | Recorded and calculated photophysical parameters of the macrocycle **1** and its precursor **2**.

	ε ($M^{-1}cm^{-1}$)	g_{lum} (P); (R_P)	g_{lum} (M); (S_P)	g_{abs}	φ	B_{CPL}
1	43 188[a]	$6{\cdot}10^{-3}$[b]	$-6{\cdot}10^{-3}$[b]	9×10^{-3}[c]	7%[b]	9[d]
2	22 579[e]	$1.3{\cdot}10^{-2}$[f]	$-1.2{\cdot}10^{-2}$[f]	$4{\cdot}10^{-3}$[g]	13%[f]	18[d]

[a]At 293 nm.
[b]At 434 nm.
[c]At 389 nm.
[d]Average of the absolute value of the g_{lum}s of both enantiomers has been considered.
[e]At 316 nm.
[f]At 396 nm.
[g]At 355 nm.

small organic molecules [33]. Interestingly, the highest g_{lum} values for the rigid macrocycle **1**, with values of $0.8{\cdot}10^{-2}$ for (*P*)-**1** and $-0.8\cdot10^{-2}$ for (*M*)-**1**, were observed at 414 nm, corresponding to the hypsochromically shifted shoulder of the maximum at 434 nm in the compounds' emission spectrum (Figure 2). At the emission maximum, the g_{lum} values are $0.6{\cdot}10^{-2}$ and $-0.6{\cdot}10^{-2}$ for (*P*)-**1** and (*M*)-**1**, respectively. The open precursor **2** shows significantly higher g_{lum} values of $1.3{\cdot}10^{-2}$ for (R_P)-**2** and $-1.2{\cdot}10^{-2}$ for (S_P)-**2** around the emission maximum at 396 nm. As g_{lum} correlates with the ratio of μm divided by μ_e, it seems that the fixation of the peripheral substituents of the chiral PCP within a helical macrocycle amplifies the electronic charge displacement during the luminescent transition more strongly (μ_e), than the enhancement in dissymmetry arising from the magnetic contribution introduced by the helical backbone (μ_m) [33].

Table 1 summarizes the photophysical properties of **1** and **2**. For enantiopure **1,** both g_{lum} and g_{abs} are in the same range ($6{\cdot}10^{-3}$ and $9{\cdot}10^{-3}$), showing a typical behavior observed for π–π* transitions where g_{abs} is usually slightly higher than their g_{lum} value [34]. In the case of **2,** on the other hand, a substantial conformational change must possibly occur upon excitation since the dissymmetry factors increase substantially from ground to excited state ($4{\cdot}10^{-3}$ and $1.2{\cdot}10^{-2}$). For both **1** and **2** the signs of the lowest energy ECD band and CPL for the same enantiomers remain the same.

With the collected data, the CPL brightness (B_{CPL}) also becomes accessible, a quantity introduced by Zinna and coworkers in 2020 to reliably describe and compare CPL emitters and to estimate their suitability for applications [35]. It is defined as:

$$B_{CPL} = \varepsilon_\lambda \times \phi \times \frac{|g_{lum}|}{2} \quad (1)$$

With ε_λ being the molar extinction coefficient, φ the total luminescence quantum yield and g_{lum} the dissymmetry factor at maximum emission. While for **1** both g_{lum} and ε_λ are relatively high, its low quantum yield of 7% leads to a quite moderate B_{CPL} of 9 $M^{-1}cm^{-1}$ compared with other PCP comprising structures [35]. The open precursor **2**, on the other hand, exhibits an extinction coefficient approximately half that of **1**, but its quantum yield is roughly twice the one of the macrocycle, as well as its g_{lum} values. These factors all lead to a higher B_{CPL} value of 18 for **2**. We are currently developing model compounds with the intention of understanding the correlation between the compact chiral structure and the resulting photophysical parameters.

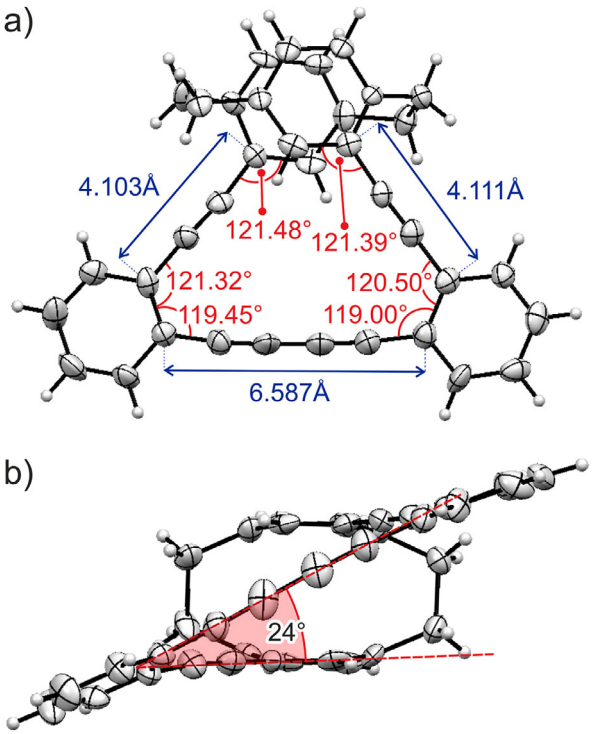

FIGURE 5 | Solid-state structure of (*P*)-**1**. (a) Top view and (b) front view.

2.3 | Solid-State Structure

In order to analyze the solid-state structure of the macrocycle **1**, several crystallization experiments were performed. Single crystals suited for x-ray diffraction experiments were obtained from a racemic mixture of **1**. By slow evaporation from a dichloromethane solution, colorless needles grew at the wall of the glass. The structure crystallizes with eight pairs of enantiomers in an orthorhombic unit cell in the non-centrosymmetric space group $Pca2_1$.

The angles of the ethynyl linkers connecting the PCP and the backbone (121.94° and 121.30°), as well as angles connected to the phenyl corners (121.32°, 120.50°, 119.45°, and 119.00°) only slightly deviate from an ideal angle of 120°, indicating low strain within the macrocycle (Figure 5a). When looking from a top view at the diacetylene backbone, a slight curvature can be observed. From the frontal perspective (Figure 5b), the backbone remains straight, oriented at 24.00° relative to the plane of the lower PCP phenyl ring.

3 | Conclusion

The compact model compound **1,** comprising a planar chiral PCP subunit forcing the macrocycle into a helical chiral arrangement, has been synthesized and separated into enantiomers by HPLC on chiral stationary phases. The pure enantiomers of the helical chiral macrocycle **1** and its planar chiral precursor **2** were analyzed with a wide range of spectroscopic techniques, providing

a comprehensive collection of spectroscopic data. While only moderate B_{CPL} values for both **1** and **2** were obtained due to low quantum yields of the compounds, the recorded g_{lum} values were impressive for small organic molecules.

The reported data provide a reliable basis for the development of model compounds to investigate correlations between structure and chiroptical features. As the synthetically accessible variations of such PCP based structure are rich and their compactness allows for efficient simulations by DFT methods, we consider the small macrocycle as ideal starting-platform for the investigation of the parameters controlling ECD and CPL on the molecular level.

4 | Experimental

4.1 | *Pseudo-Ortho* Dibromo PCP 6

Literature-known *pseudo-para* dibromo PCP [36] (10.0 g, 27.3 mmol, 1.0 eq.) was suspended in *ortho*-dichlorobenzene in a microwave tube. The mixture was heated to 200°C, stirred for 5 min, and then let come to room temperature. The solids were filtered off, water was added, and solvents were removed under reduced pressure. Water was added continuously to help with the evaporation of *ortho*-dichlorobenzene. The remaining solids were subjected to column chromatography (350 g SiO_2, CH/CH_2Cl_2 (95:5)) to give **6** (7.65 g, 20.9 mmol, 77%) as a white solid. The analytical data are consistent with literature values [37].

^{1}H NMR (400 MHz, $CDCl_3$) δ 7.19 (d, J = 1.7 Hz, 1H), 6.67–6.40 (m, 2H), 3.45 (ddd, J = 13.3, 9.5, 2.3 Hz, 1H), 3.24–2.97 (m, 2H), 2.81 (ddd, J = 13.3, 10.1, 7.0 Hz, 1H).

4.2 | *Pseudo-Ortho* Bis(TMS-Ethynyl) PCP 5

To **6** (200 mg, 0.55 mmol, 1.0 eq.) dissolved in a degassed THF/TEA (20 mL, 1:1) mixture $Pd_2(dba)_3$ (14.9 mg, 13.3 µmol, 3.0 mol%), $[(t\text{-}Bu)_3PH]BF_4$ (19.1 mg, 12 µmol, 12 mol%) and CuI (3.12 mg, 16.3 µmol, 3 mol%) were added and the solution was degassed for 5 min more. Trimethylsilylacetylene (0.13 mL, 0.92 mmol, 4.0 eq.) was added, and the mixture was placed in a preheated oil bath at 50°C for 16 h. Solvents were evaporated, and the crude was subjected to column chromatography (50 g SiO_2, CH) to give **5** (160 mg, 0.40 mmol, 73%) as a brown oil.

^{1}H NMR (500 MHz, $CDCl_3$) δ 7.04 (d, J = 1.8 Hz,18.8 2H), 6.53–6.38 (m, 4H), 3.57 (ddd, J = 12.8, 10.4, 2.3 Hz, 2H), 3.11 (ddd, J = 13.1, 10.5, 6.0 Hz, 2H), 3.02 (ddd, J = 12.8, 10.4, 2.3 Hz, 2H), 2.78 (ddd, J = 13.1, 10.5, 6.0 Hz, 2H), 0.32 (s, 18H). **^{13}C NMR** (126 MHz, $CDCl_3$) δ 142.8, 139.6, 134.1, 133.6, 133.3, 124.8, 105.5, 97.8, 34.5, 33.4, 0.3. **HRMS (ESI-ToF)**: calc. for $C_{26}H_{33}Si_2$ 401.2115 $[M + H]^+$; found 401.2115, calc. for $C_{26}H_{32}AgSi_2$ 507.1088 $[M + Ag]^+$; found 507.1088.

4.3 | *Pseudo-Ortho* Diacetylene PCP 4

5 (160 mg, 0.40 mmol, 1.0 eq.) and K_2CO_3 (552 mg, 4.0 mmol, 10. eq.) were dissolved in a methanol/CH_2Cl_2 (1:1 4 mL) mixture and let stir for 24 h at room temperature. Solvents were evaporated under reduced pressure, and the residue was transferred to a separation funnel via EtOAc and water and extracted with EtOAc (3x). The combined organic phases were dried over Na_2SO_4, and the solvents were removed in vacuo. The crude was subjected to column chromatography (25 g, SiO_2, CH) to give **4** (75 mg, 0.29 mmol, 73%) as a yellow liquid that solidified upon standing. The analytical data are consistent with literature values [22].

^{1}H NMR (400 MHz, $CDCl_3$) δ 7.07 (d, J = 1.8 Hz, 2H), 6.62–6.41 (m, 4H), 3.58 (ddd, J = 12.7, 9.9, 2.5 Hz, 2H), 3.30 (s, 2H), 3.22–2.97 (m, 4H), 2.82 (ddd, J = 13.1, 10.2, 6.1 Hz, 2H). **^{13}C NMR** (101 MHz, $CDCl_3$) δ 142.9, 139.7, 134.6, 133.7, 133.6, 123.8, 83.5, 80.6, 34.3, 33.4. **HRMS (ESI-ToF)**: calc. for $C_{20}H_{17}$ 257.1325 $[M + H]^+$; found 257.1324, calc. for $C_{22}H_{20}N$ 298.1590 $[M + ACN + H]^+$; found 298.1590 calc. for $C_{20}H_{16}Ag$ 363.0297 $[M + Ag]^+$; found 363.0299, calc. for $C_{40}H_{33}$ 513.2577 $[2M + H]^+$; found 513.2572.

4.4 | PCP Dialdehyde 3

A round bottom flask flushed three times with argon was loaded with **4** (45 mg, 0.18 mmol, 1.0 eq.), $Pd(PPh_3)_2Cl_2$ (12.3 mg, 17.3 µmol, 0.1 eq.), CuI (3.31 mg, 17.3 µmol, 0.1 eq.), and PPh_3 (9.08 mg, 34.6 µmol, 0.2 eq.). A degassed solution of *ortho*-bromobenzaldehyde (128 mg, 0.69 mmol, 4.0 eq.) in THF/TEA (1:4, 10 mL) was added, and the reaction mixture was put in a preheated oil bath at 70°C and stirred for 20 h. Solvents were evaporated and the crude was subjected to column chromatography (25 g, SiO_2, CH:EtOAc 1:0→ 95:5) to give dialdehyde **3** (31 mg, 66.7 µmol, 39%) as a white powder.

^{1}H NMR (400 MHz, $CDCl_3$) δ 10.84 (s, 2H), 8.10 (dd, J = 7.8, 1.5 Hz, 2H), 7.81 (dd, J = 7.7, 1.4 Hz, 2H), 7.74 (td, J = 7.5, 1.5 Hz, 2H), 7.65–7.56 (m, 2H), 7.38 (s, 2H), 6.74 (m, 4H), 3.79 (ddd, J = 13.1, 10.1, 2.9 Hz, 2H), 3.39–3.19 (m, 4H), 3.10 (ddd, J = 13.1, 10.2, 6.0 Hz, 2H). **^{13}C NMR** (101 MHz, $CDCl_3$) δ 191.5, 142.7, 140.0, 135.9, 134.6, 134.1, 134.1, 134.0, 133.7, 128.7, 127.8, 127.2, 124.1, 96.4, 88.8, 34.6, 34.0. **HRMS (ESI-ToF)**: calc. for $C_{34}H_{25}O_2$ 465.1849 $[M + H]^+$; found 465.1858, calc. for $C_{34}H_{24}NaO_2$ 482.2115 $[M + Na]^+$; found 482.2115.

4.5 | Diacetylene 2

An oven-dried round-bottom flask was loaded with **3** (25 mg, 35.8 µmol, 1.0 eq.) Cs_2CO_3 (140 mg, 0.43 mol, 8.0 eq.), flushed with argon (3x), and MeOH (dry, 3.3 mL) and THF (dry, 3.3 mL) were added. Ohira–Bestmann reagent (17.8 µL, 0.12 mmol, 2.2 eq.) was added, and the reaction mixture was heated to 50°C and stirred until full conversion was observed (TLC control after 10 min). Water was added, and MeOH was removed in vacuo. HCl (1 M) was added, and the mixture was extracted with EtOAc (3 x); the solvents were evaporated under reduced pressure. The residue was filtered through a silica plug (CH/EtOAc 8:2) to give **2** (19 mg, 41.6 µmol, 77%) as a brown oil.

^{1}H NMR (500 MHz, $CDCl_3$) δ 7.61–7.52 (m, 4H), 7.38–7.26 (m, 4H), 7.25 (d, J = 1.1 Hz, 2H), 6.57 (d, J = 1.1 Hz, 4H), 3.83 (ddd, J = 12.8, 10.5, 2.2 Hz, 2H), 3.36 (s, 2H), 3.34–3.28 (m, 2H), 3.07 (ddd, J = 13.0, 10.6, 2.2 Hz, 2H), 2.88 (ddd, J = 13.0, 10.5, 5.7 Hz, 2H).

^{13}C NMR (126 MHz, $CDCl_3$) δ 142.6, 139.9, 134.6, 133.7, 133.5, 132.9, 132.3, 128.7, 127.8, 127.2, 124.8, 124.4, 93.7, 91.4, 82.7, 81.4, 34.6, 33.7.

HRMS (ESI-ToF): calc. for $C_{36}H_{24}Ag$ 463.0923 $[M + Ag]^+$; found 563.0931.

4.6 | PCP Macrocycle 1

A round bottom flask **2** (9.1 mg, 19.9 µmol, 1.0 eq.) was dissolved in pyridine (3 mL) and was heated to 80°C in an oil bath. $CuOAc{\cdot}H_2O$ (39.8 mg, 199 µmol, 10 eq.) was added, and the reaction was stirred for 1 h at this temperature. Solvents were removed under reduced pressure, and the crude reaction was subjected to column chromatography (10 g, SiO_2, CH:EtOAc 1:0→ 9:1) to give **1** (7.0 mg, 15.4 19.9 µmol, 77.3%) as a white solid. The analytical data are consistent with literature values [22].

^{1}H NMR (500 MHz, CD_2Cl_2) δ 7.61 – 7.52 (m, 4H), 7.42-7.05 (m, 4H), 7.05 (s, 2H), 6.67 – 6.62 (m, 4H), 3.76 – 3.68 (m, 2H), 3.20 – 3.02 (m, 4H), 2.89-2.89 (m, 2H). **^{13}C NMR** (126 MHz, CD_2Cl_2) δ 144.0, 140.4, 134.3, 134.0, 133.7, 132.8, 131.4, 129.5, 129.3, 128.4, 124.1, 123.8, 94.0, 91.3, 82.5, 78.7, 35.9, 33.6, 30.1.

HRMS (ESI-ToF): calc. for $C_{36}H_{22}$ Ag 561.0767 $[M + Ag]^+$; found 561.0767.

Author Contributions

S.L.H. conceptualized the project; synthesized the compounds, performed computations, measured UV–vis, Fluorescence, and ECD spectra, and wrote the manuscript; A.D'A. measured CPL. O.F. and D.F. analyzed the solid-state structures; M. M. supervised the work and wrote the manuscript. All authors commented on the manuscript.

Acknowledgments

We thank Prof. Dr. M. Pittelkow and the Danish Council for Independent Research (DFF Grant Number. 4181-00206 and 9040-00265) for access to the CPL Spectrometer. We thank Michael Zengaffinen for measuring quantum yields.

The authors acknowledge generous support by the Swiss National Science Foundation (SNF Grant no. 200020–207744). M.M. acknowledges support from the 111 project (Grant No. 90002–18011002). Open Access funding provided by Universität Basel.

Open access publishing facilitated by Universitat Basel, as part of the Wiley - Universitat Basel agreement via the Consortium Of Swiss Academic Libraries.

Conflicts of Interest

The authors declare no conflicts of interest.

Data Availability Statement

The data that support the findings of this study are available in the Supporting Information of this article.

References

1. M. Rickhaus, M. Mayor, and M. Juríček, "Chirality in Curved Polyaromatic Systems," *Chemical Society Reviews* 46 (2017): 1643–1660, https://doi.org/10.1039/C6CS00623J.

2. M. Rickhaus, M. Mayor, and M. Juríček, "Strain-induced Helical Chirality in Polyaromatic Systems," *Chemical Society Reviews* 45 (2016): 1542–1556, https://doi.org/10.1039/C5CS00620A.

3. L. D. Bizzini, T. Müntener, D. Häussinger, M. Neuburger, and M. Mayor, "Synthesis of Trinorbornane," *Chemical Communications* 53 (2017): 11399–11402, https://doi.org/10.1039/C7CC06273G.

4. L. D. Bizzini, T. Bürgi, and M. Mayor, "The Enantiomers of Trinorbornane and Derivatives Thereof," *Helvetica Chimica Acta* 103 (2020): e2000019.

5. E. Sidler, J. Malinčík, A. Prescimone, and M. Mayor, "Induced Axial Chirality by a Tight Belt: Naphthalene Chromophores Fixed in a 2,5-substituted Cofacial Para-Phenylene–Ethynylene Framework," *Journal of Materials Chemistry* 9 (2021): 16199–16207.

6. D. Vonlanthen, J. Rotzler, M. Neuburger, and M. Mayor, "Synthesis of Rotationally Restricted and Modular Biphenyl Building Blocks," *European Journal of Organic Chemistry* 2010 (2010): 120–133, https://doi.org/10.1002/ejoc.200900805.

7. M. Rickhaus, L. M. Bannwart, M. Neuburger, et al., "Inducing Axial Chirality in a "Geländer" Oligomer by Length Mismatch of the Oligomer Strands," *Angewandte Chemie International Edition* 53 (2015): 14587–14591, https://doi.org/10.1002/anie.201408424.

8. M. Rickhaus, L. M. Bannwart, O. Unke, H. Gsellinger, D. Häussinger, and M. Mayor, "Through the Maze: Cross-Coupling Pathways to a Helical Hexaphenyl "Geländer" Molecule," *European Journal of Organic Chemistry* 2015 (2015): 786–801, https://doi.org/10.1002/ejoc.201403322.

9. R. Mannancherry, M. Rickhaus, D. Häussinger, A. Prescimone, and M. Mayor, "Molecular Dynamic Staircases: All-Carbon Axial Chiral "Geländer" Structures," *Chemical Science* 9 (2018): 5758–5766, https://doi.org/10.1039/C8SC01707G.

10. L. M. Bannwart, L. Jundt, T. Müntener, M. Neuburger, D. Häussinger, and M. Mayor, "A Phenyl-Ethynyl-Macrocycle: A Model Compound for "Geländer" Oligomers Comprising Reactive Conjugated Banisters," *European Journal of Organic Chemistry* 2018 (2018): 3391–3402, https://doi.org/10.1002/ejoc.201800586.

11. H. Dekkiche, J. Malinčik, A. Prescimone, D. Häussinger, and M. Mayor, "An Ortho-Tetraphenylene-Based "Geländer" Architecture Consisting Exclusively of 52 sp^2-Hybridized C Atoms," *Chemistry – A European Journal* 27 (2021): 13258–13267.

12. L. M. Bannwart, T. Müntener, M. Rickhaus, L. Jundt, D. Häussinger, and M. Mayor, "Bicyclic Phenyl–Ethynyl Architectures: Synthesis of a 1,4-Bis(phenylbuta-1,3-diyn-1-yl) Benzene Banister," *Chemistry – A European Journal* 27 (2021): 6295–6307.

13. R. Mannancherry, T. Šolomek, D. Cavalli, et al., "Sulfone "Geländer" Helices: Revealing Unexpected Parameters Controlling the Enantiomerization Process," *Journal of Organic chemistry* 86 (2021): 5431–5442.

14. A. D'Addio, J. Malinčik, O. Fuhr, D. Fenske, D. Häussinger, and M. Mayor, "Geländer Molecules With Orthogonal Joints: Synthesis of Macrocyclic Dimers," *Chemistry – A European Journal* 28 (2022): e202201678.

15. A. D'Addio, C. C. E. Kroonen, O. Fuhr, D. Fenske, D. Häussinger, and M. Mayor, "Series of Geländer Oligomers With Orthogonal Rungs," *Chemical Science* 16 (2025): 8092–8098.

16. C. C. E. Kroonen, A. D'Addio, A. Prescimone, D. Häussinger, and M. Mayor, "A Cross-Shaped Organic Framework: A Multi-functional Template Arranging Chromophores," *Organic Chemistry Frontiers* 12 (2025): 1399–1408, https://doi.org/10.1039/D4QO01808G.

17. C. C. E. Kroonen, A. D'Addio, A. Prescimone, O. Fuhr, D. Fenske, and M. Mayor, "A Cross-Shaped Monomer as Building Block for Molecular Textiles," *Helvetica Chimica Acta* 106 (2023): e202200204, https://doi.org/10.1002/hlca.202200204.

18. K. J. Weiland, T. Brandl, K. Atz, et al., "Mechanical Stabilization of Helical Chirality in a Macrocyclic Oligothiophene," *Journal of the American Chemical Society* 141 (2019): 2104–2110, https://doi.org/10.1021/jacs.8b11797.

19. K. J. Weiland, N. Münch, W. Gschwind, D. Häussinger, and M. Mayor, "A Chiral Macrocyclic Oligothiophene With Broken Conjugation—Rapid Racemization Through Internal Rotation," *Helvetica Chimica Acta* 102 (2019): e1800205, https://doi.org/10.1002/hlca.201800205.

20. E. Sidler, P. Zwick, C. Kress, et al., "Intense Molar Circular Dichroism in Fully Conjugated All-Carbon Macrocyclic 1,3-Butadiyne Linked Pseudo- Meta [2.2]Paracyclophanes**," *Chemistry—A European Journal* 28 (2022): e202201764, https://doi.org/10.1002/chem.202201764.

21. C. Kress, E. Sidler, P. Downey, et al., "Circularly Polarized Luminescence of Thiophene-Bridged Macrocyclic Pseudo-Meta [2.2]Paracyclophanes," *Chemistry – A European Journal* 30 (2024): e202303798.

22. H. Hinrichs, A. J. Boydston, P. G. Jones, et al., "Phane Properties of [2.2]Paracyclophane/Dehydrobenzoannulene Hybrids," *Chemistry – A European Journal* 12 (2006): 7103–7115.

23. A. J. Boydston, L. Bondarenko, I. Dix, T. J. R. Weakley, H. Hopf, and M. M. Haley, "[2.2]Paracyclophane/Dehydrobenzoannulene Hybrids: Transannular Delocalization in Open-Circuited Conjugated Macrocycles," *Angewandte Chemie International Edition* 40 (2001): 2986–2989.

24. K. Sugiura, "[2.2]Paracyclophane-Based Chiral Platforms for Circularly Polarized Luminescence Fluorophores and Their Chiroptical Properties: Past and Future," *Frontiers in Chemistry* 8 (2020): 2296–2646, https://doi.org/10.3389/fchem.2020.00700.

25. Z. Hassan, E. Spuling, D. M. Knoll, J. Lahann, and S. Bräse, "Planar Chiral [2.2]Paracyclophanes: From Synthetic Curiosity to Applications in Asymmetric Synthesis and Materials," *Chemical Society Reviews* 47 (2018): 6947–6963, https://doi.org/10.1039/C7CS00803A.

26. Z. Hassan, E. Spuling, D. M. Knoll, J. Lahann, and S. Bräse, "Regioselective Functionalization of [2.2]Paracyclophanes: Recent Synthetic Progress and Perspectives," *Angewandte Chemie International Edition* 59 (2020): 2156–2170, https://doi.org/10.1002/anie.201904863.

27. Y. Moriskai, M. Gon, T. Sasamori, N. Tokitoh, and Y. Chujo, "Planar Chiral Tetrasubstituted [2.2] Paracyclophane: Optical Resolution and Functionalization," *Journal of the American Chemical Society* 136 (2014): 3350–3353, https://doi.org/10.1021/ja412197j.

28. K. Matsamura, R. Inoue, and Y. Morisaki, "Optically Active A-Shaped Cyclic Molecules Based on Planar Chiral [2.2]Paracyclophanes Emitting Bright Circularly Polarized Luminescence With High Anisotropy Factors," *Advanced Functional Materials* 34, no. 136 (2024): 2310566, https://doi.org/10.1002/adfm.202310566.

29. H. J. Reich and D. J. Cram, "Macro Rings. XXXVI. Ring Expansion, Racemization, and Isomer Interconversions in the [2.2]Paracyclophane System Through a Diradical Intermediate," *Journal of the American Chemical Society* 91 (1969): 3517–3526, https://doi.org/10.1021/ja01041a016.

30. F. Neese, "Software Update: The ORCA Program System—Version 5.0.0," *WIREs Computational Molecular Science* 12 (2022): e1606, https://doi.org/10.1002/wcms.1606.

31. F. Neese, "An Improvement of the Resolution of the Identity Approximation for the Formation of the Coulomb Matrix," *Journal of Computational Chemistry* 24 (2003): 1740–1747, https://doi.org/10.1002/jcc.10318.

32. F. Neese, F. Wennmohs, A. Hansen, and U. Becker, "Efficient, Approximate and Parallel Hartree–Fock and Hybrid DFT Calculations. A 'Chain-of-Spheres' Algorithm for the Hartree–Fock Exchange," *Chemical Physics* 356 (2009): 98–109, https://doi.org/10.1016/j.chemphys.2008.10.036.

33. C. A. Guido, F. Zinna, and G. Pescitelli, "Quantum Chemistry Calculations of Circularly Polarized Luminescence (CPL): From Spectral Modeling to Molecular Design," *Chemical Reviews* 125 (2025): 10492–10656.

34. H. Tanaka, Y. Inoue, and T. Mori, "Circularly Polarized Luniescence and Circular Dichroism in Small Organic Molecules: Correlation Between Excitation and Emission Dissymmetry Factors," *ChemPhotoChem* 2 (2018): 386–402.

35. L. Arrico, L. D. Bari, and F. Zinna, "Quantifying the Overall Efficiency of Circularly Polarized Emitters," *Chemistry – A European Journal* 27 (2021): 2920–2934.

36. N. V. Vorontsova, V. I. Rozenberg, E. V. Sergeeva, et al., "Symmetrically Tetrasubstituted [2.2]Paracyclophanes: Their Systematization and Regioselective Synthesis of Several Types of Bis-Bifunctional Derivatives by Double Electrophilic Substitution," *Chemistry – A European Journal* 14 (2008): 4600–4617.

37. B. König, B. Knieriem, and A. de Meijere, "Double-Layered 1,4-Distyrylbenzene Chromophores—Synthesis, UV and Fluorescence Spectra," *Chemische Berichte* 126 (1993): 1643–1650.

38. O. V. Dolomanov, L. J. Bourhis, R. J. Gildea, J. K. Howard, and H. Puschmann, "Complete Structure Solution, Refinement and Analysis Program," *Journal of Applied Crystallography* 42 (2009): 339–341, https://doi.org/10.1107/S0021889808042726.

39. G. M. Sheldrick, "SHELXT – Integrated space-group and Crystalstructure Determination," *Acta Crystallographica Section A, Foundations and Advances* 71 (2015): 3–8, A71.

40. G. M. Sheldrick, "Crystal Structure Refinement With SHELXL," *Acta Crystallographica Section C, Structural Chemistry* 71 (2015): 3–8, C71.

Supporting Information

Additional supporting information can be found online in the Supporting Information section.

The authors have cited additional references within the Supporting Information [36–40].

Supporting File: hlca70078-sup-0001-SuppMat.pdf.